The Journal of Immunology

Structural and Biological Basis of CTL Escape in Coronavirus-Infected Mice

Noah S. Butler, Alex Theodossis, Andrew I. Webb, Michelle A. Dunstone, Roza Nastovska, Sri Harsha Ramarathinam, Jamie Rossjohn, Anthony W. Purcell and Stanley Perlman

J Immunol 2008; 180:3926-3937; ;
doi: 10.4049/jimmunol.180.6.3926
http://www.jimmunol.org/content/180/6/3926

The Journal of Immunology is published twice each month by
The American Association of Immunologists, Inc.,
9650 Rockville Pike, Bethesda, MD 20814-3994.

Print ISSN: 0022-1767 Online ISSN: 1550-6606.

Structural and Biological Basis of CTL Escape in Coronavirus-Infected Mice[1]

Noah S. Butler,[2]*† Alex Theodossis,[2]‡ Andrew I. Webb,§ Michelle A. Dunstone,‡ Roza Nastovska,§ Sri Harsha Ramarathinam,§ Jamie Rossjohn,‡ Anthony W. Purcell,[3]§ and Stanley Perlman[3]*†

Cytotoxic T lymphocyte escape occurs in many human infections, as well as mice infected with the JHM strain of mouse hepatitis virus, which exhibit CTL escape variants with mutations in a single epitope from the spike glycoprotein (S510). In all CTL epitopes prone to escape, only a subset of all potential variants is generally detected, even though many of the changes that are not selected would result in evasion of the T cell response. It is postulated that these unselected mutations significantly impair virus fitness. To define more precisely the basis for this preferential selection, we combine x-ray crystallographic studies of the MHC class I (D^b)/S510 complexes with viral reverse genetics to identify a prominent TCR contact residue (tryptophan at position 4) prone to escape mutations. The data show that a mutation that is commonly detected in chronically infected mice (tryptophan to arginine) potently disrupts the topology of the complex, explaining its selection. However, other mutations at this residue, which also abrogate the CTL response, are never selected in vivo even though they do not compromise virus fitness in acutely infected animals or induce a significant de novo CTL response. Thus, while structural analyses of the S510/D^b complex provide a strong basis for why some CTL escape variants are selected, our results also show that factors other than effects on virus fitness limit the diversification of CD8 T cell epitopes. *The Journal of Immunology,* **2008, 180: 3926–3937.**

Cytotoxic T lymphocytes recognize viral Ags displayed on the surface of infected cells in the context of MHC class I (reviewed in Ref. 1). CTL that recognize their cognate Ags are critically important for eliminating virus-infected cells. The resultant immune pressure can result in the selective outgrowth of viruses that have undergone mutation in targeted, immunodominant CD8 T cell epitopes. These CTL escape viruses contribute to enhanced pathogenesis and disease progression (2, 3). Such escape viruses have been identified in humans infected with HIV and hepatitis C virus (HCV)[4], and in nonhuman primates infected with SIV and HCV (reviewed in Ref. 4). CTL escape in HIV-infected patients has been associated with progression to AIDS (5). Sequential mutation of CD8 T cell epitopes in nonhuman primates infected with HCV is also strongly associated with persistent infection and disease progression (6). Although these data provide strong evidence for the clinical relevance of CTL escape, only some CD8 T cell epitopes undergo escape and, within individual epitopes, specific residues are mutated preferentially. The limited variability of certain CD8 T cell epitopes is postulated to reflect the functional constraints of mutation on virus fitness, although this has not been directly demonstrated in vivo (7–11). Other factors may also contribute to the selection of a limited subset of CTL escape viruses, such as the development of de novo CD8 T cell responses (12–14) and cross-recognition of variant epitopes by existing CTL, which has been described in the setting of HIV infection (15). Furthermore, and paradoxically, CTL escape is sometimes detected in the presence of a robust immune response, without resulting in apparent enhancement of virus replication or disease progression. Perhaps the best example of this is shown in HIV-infected HLA-B57 and HLA-B*5801-positive individuals, in which mutation in a dominant CTL epitope, TW10, commonly occurs but is not associated with progression to AIDS (16–18). Likewise, SIV-infected rhesus monkeys expressing

*Department of Microbiology and †Immunology Graduate Program, University of Iowa, Iowa City, IA 52242; ‡The Protein Crystallography Unit, Department of Biochemistry and Molecular Biology, School of Biomedical Sciences, Monash University, Clayton; and §Department of Biochemistry and Molecular Biology, Bio21 Molecular Science and Biotechnology Institute, University of Melbourne, Parkville, Victoria, Australia

Received for publication November 6, 2007. Accepted for publication January 5, 2008.

The costs of publication of this article were defrayed in part by the payment of page charges. This article must therefore be hereby marked *advertisement* in accordance with 18 U.S.C. Section 1734 solely to indicate this fact.

[1] This work was supported by National Institutes of Health Grant R01 NS036592-09 (to S.P. and A.W.P.), and a National Institutes of Health Predoctoral Training Grant on Mechanisms of Parasitism (T32 AI007511 to N.S.B.). A.W.P. is a Senior Research Fellow, M.A.D. is a Doherty Post-doctoral Fellow, and A.I.W. is a C. J. Martin Fellow of the National Health and Medical Research Council of Australia. J.R. is an Australian Research Council Federation Fellow.

[2] N.B. and A.T. contributed equally to this work.

[3] Address correspondence and reprint requests to Dr. Stanley Perlman, Department of Microbiology, Bowen Science Building 3-712, University of Iowa, Iowa City, IA 52242. E-mail address: Stanley-perlman@uiowa.edu or Dr. Anthony Purcell, Department of Biochemistry and Molecular Biology, The Bio21 Molecular Science and Biotechnology Institute, University of Melbourne, 3010 Victoria, Australia. E-mail address: apurcell@unimelb.edu.au

[4] Abbreviations used in this paper: HCV, hepatitis C virus; JHMV, JHM strain of mouse hepatitis virus; S510, the immunodominant H-2D^b-restricted epitope from the spike glycoprotein of JHMV (CSLWNGPHL); S598, subdominant H-2K^b-restricted epitope spanning residues 598–605 of the spike glycoprotein of JHMV (RCQIFANI); p.i., postinfection; Aba, L-α aminobutyric acid; W513R, position 4 Arg-substituted S510 epitope (CSLRNGPHL); W513G, position 4 Gly-substituted S510 epitope (CSLGNGPHL); W513S, position 4 Ser-substituted S510 epitope (CSLSNGPHL); W513L, position 4 Leu-substituted S510 epitope (CSLLNGPHL); PEG, polyethylene glycol; rJ, recombinant JHMV; rJ.S_{W513G}, recombinant JHMV bearing the W513G mutation introduced by reverse genetics; rJ.S_{W513S}, recombinant JHMV bearing the W513S mutation introduced by reverse genetics; rJ.S_{W513L}, recombinant JHMV bearing the W513L mutation introduced by reverse genetics; rJ.S_{W513R}, recombinant JHMV bearing the W513R mutation introduced by reverse genetics; MOI, multiplicity of infection; WT, wild type; OVA, chicken ovalbumin; DC, dendritic cell; CD, circular dichroism; T_m, midpoint of thermal denaturation; rmsd, root mean square deviation; LCMV, lymphocytic choriomeningitis virus; HGV, hepatitis G virus.

Table I. *CTL escape mutations identified in mice persistently infected with MHV strain JHM*[a]

Single Residue Mutations			
Position	Residue	Variants Recovered (Frequency)[b]	Total
1	C	None	0
2	S	F (40%), P (30%), Y (20%), T (10%)	10
3	L	F (58%), R (24%), P (14%), W (4.5%)	21
4	W	R (89%), G (7.7%)[c], C (3.3%)[d]	26
5	N	S (59%), K (17%), D (14.4%), T (4.8%), H (2.4%), Y (2.4%)	41
6	G	R (50%), V (28.6%), E (14.3%), W (7.1%)	14
7	P	L (76.2%), H (14.3%), S (9.5%)	19
8	H	None	0
9	L	None	0
Residue deletions: Change of			
S			1
L			1
W			2
SL → F			6
SL			3
LWN			1
Entire epitope			40
Total variants			187

[a] Refs. 22, 27–29.
[b] Proportion of variant changes detected at each position.
[c] W513G was detected in two asymptomatic mice and represented <30% of the variant virus quasispecies within each mouse.
[d] W513C was detected in one symptomatic mouse and represented <30% of the variant virus quasispecies.

Mamu-A*01 progress to AIDS more slowly than do monkeys expressing other MHC class I haplotypes (19, 20), despite frequent escape in a well-defined immunodominant CD8 T cell epitope, CM9, restricted by Mamu-A*01. The obvious explanation for these observations is that virus fitness has been compromised by mutation in TW10 and CM9 epitopes. Consistent with this, these mutations occur early in the infection, but variant virus is not predominant until disease progression occurs, and at least in the case of CM9, epitope variants are only selected in the presence of a second compensatory mutation that restores viral core assembly to wild-type (WT) levels (4, 20, 21).

Because CTL escape variant viruses are most commonly detected only in humans infected with HIV or HCV, and in nonhuman primates infected with SIV, mutational effects on virus fitness or prospective studies of de novo CD8 T cell responses that may suppress CTL escape variant virus replication are difficult or impossible to test in vivo. Thus, current data that define the basis for the selection of CTL escape variant viruses are, in large part, correlative. CTL escape also commonly occurs in C57BL/6 (B6) mice persistently infected with neurovirulent mouse hepatitis virus strain JHM (JHMV) and correlates with disease progression (22, 23). In these studies, suckling mice are inoculated with virus and nursed by JHMV-immune dams, resulting in maternal Ab-mediated protection from lethal acute encephalitis. However, between days 21 and 60 postinfection (p.i.), a proportion of mice develop hindlimb paresis/paralysis and demyelination on histological examination. Infectious virus is present in mice with clinical disease and is mutated in the immunodominant epitope S510 (spanning residues 510–518 of the spike (S) glycoprotein, CSLWNGPHL, H-2D^b-restricted). A subdominant CD8 T cell epitope from the same Ag (epitope S598, spanning residues 598–605 of the S glycoprotein, RCQIFANI, H-2K^b-restricted) is never mutated. In contrast to human and nonhuman primate infections, this murine model is easily manipulable, and reverse-genetic approaches allow the introduction of mutations into the JHMV genome (24), allowing in vivo testing of mutated viruses. Importantly, mutations are detected within epitope S510, facilitating direct in vitro and in vivo studies of the mechanisms of CTL escape.

As in humans or nonhuman primates infected with HCV, HIV, or SIV (10, 11, 25, 26), only a limited subset of possible CTL escape mutations in epitope S510 are detected in mice persistently infected with JHMV (22, 27–29). There is also selectivity within the set of mutations observed at a given residue. For example, almost 90% of CTL escape variants at position 4 of the S510 epitope (Wp4) are tryptophan to arginine substitutions (W513R) (Table I). These apparent constraints on antigenic plasticity are not predicted, as the region of the spike glycoprotein encoding epitope S510 is prone to mutation and deletion (reviewed in Ref. 30). Thus, the basis for the selection of a limited subset of CTL escape variant viruses in mice persistently infected with JHMV is unclear.

Herein, we have solved the crystal structure of the H-2D^b/S510 complex to gain insight into how specific mutations in the epitope abrogate recognition by CD8 T cells. CTL escape is observed in both MHC-anchoring residues and TCR-accessible residues. However, of the two most prominent solvent-accessible residues, only the tryptophan at position 4 is observed to generate escape variants. Molecular virological and immunological studies have been used to dissect out the basis of the near complete bias of tryptophan to arginine substitution at this position in escape variants isolated from afflicted mice.

Materials and Methods

X-ray crystallographic studies

Crystals of H-2D^{b}S510-Aba were grown at 21°C in 0.1 M of citrate (pH 7.5), 28% polyethylene glycol (PEG) 3350, and 0.2 M of $LiSO_4$ using a protein concentration of 3 mg/ml. Crystals were cryoprotected by equilibration against mother liquor containing 5% glycerol and flash frozen by placement in a nitrogen stream. The 2.1 Å dataset were collected at the Advanced Photon Source (Chicago, IL) synchrotron facility. Crystals of H-2D^{b}S510$_{W513S}$-Aba were grown at 21°C in 0.1 M of citrate (pH 6.4), 28% PEG 3350, and 0.15 M of $LiSO_4$ using a protein concentration of 6 mg/ml. Crystals were cryoprotected using perfluoropolyether

Table II. *Data collection and refinement statistics*

Structure	H-2D^{b}S510-Aba	H-2D^{b}S510-W513S-Aba
Wavelength (Å)	1.0	1.0
Resolution limits (Å)[a]	58.00–2.10 (2.21–2.10)	34.00–2.70 (2.85–2.70)
Space group	$P2_1$	$P2$
Unit-cell parameters (Å)	$a = 79.54$, $b = 86.06$, $c = 152.07$ $\beta = 90.01°$	$a = 83.56$, $b = 71.03$, $c = 87.00$ $\beta = 103.45°$
No. observations	317,766	81,387
No. unique reflections	113,937	27,219
Mosaicity	0.22	0.65
Completeness (%)[a]	95.4 (97.3)	99.3 (99.1)
R_{merge} (%)[a,b]	5.6 (18.5)	8.3 (33.0)
$\langle I/\sigma(I)\rangle$[a]	13.5 (4.8)	12.7 (3.2)
Multiplicity[a]	2.8 (2.7)	3.0 (3.0)
R_{factor} (%)[c]	20.3	25.3
R_{free} (%)[d]	26.1	30.6
No. of atoms		
Protein[e]	11,803 (28.4)	5,821 (27.0)
Peptide[e]	288 (16.9)	128 (14.6)
Water[e]	986 (33.7)	118 (21.2)
Other[e]	30 (16.4)	5 (25.2)
rmsd bonds (Å)	0.020	0.006
rmsd angles (°)	1.79	0.993

[a] Values in parentheses refer to the highest resolution bin.
[b] $R_{merge} = \Sigma_{hkl}\Sigma_i|I_{hkl,i} - \langle I_{hkl}\rangle|/\Sigma_{hkl}\langle I_{hkl}\rangle$.
[c] $R_{factor} = (\Sigma||F_o| - |F_c||)/(\Sigma|F_o|)$ - for all data except as indicated in footnote d.
[d] 5% of data was used for the R_{free} calculation (see footnote c).
[e] Values in parentheses indicate the average B-factor (in units Å^2) for all atoms.

before flash freezing. The 2.7-Å dataset was collected at the Australian Synchrotron Facility in Melbourne, Australia. In both cases the data were integrated in Mosflm (31) and scaled/merged using Scala (32). The structures were solved by molecular replacement in Phaser (33) against a previously solved H-2D^b complex (PDBid: 1BZ9). The resulting models were subjected to iterative cycles of refinement in Refmac5 (34), followed by model building/correction in Coot (35). The solvent structures were built using ARP/wARP (36) and then Coot. A summary of the processing and refinement statistics is presented in Table II.

Viruses

Recombinant, WT, and epitope S510 variants of JHMV were generated using overlapping extension PCR as previously described (24, 37). Primers that overlapped the tryptophan at residue 513 of the spike glycoprotein were (5′ to 3′) W513G: fwd, GTGAGTGTTCTCTTGGGAATGGGCCCCATTTGCGCTCGGC, rev, AGCGCAAATGGGGCCCATTCCCAAGAGAACACTCAC; W513L: fwd, GTGAGTGTTCTCTTTTGAATGGGCCCCATTTGCGCTCGGC,rev,AGCGCAAATGGGGCCCATTCAAAAGAGAACACTCAC; W513S: fwd, GTGAGTGTTCTCTTTCGAATGGGCCCCATTTGCGCTCGGC, rev, AGCGCAAATGGGGCCCATTCGAAAGAGAACACTCAC; W513R: fwd, GTGAGTGTTCTCTTCGGAATGGGCCCCATTTGCGCTCGGC,rev,AGCGCAAATGGGGCCCATTCCGAAGAGAACACTCAC. The outer primers were fwd, TGTTGATTGCGCCAGCAGCTACATTAG; and rev, ACCTACGGATTGAACGCTATCATTGAC. Recombinant viruses encoding variant S510 epitopes (rJ.S$_{W513G}$, rJ.S$_{W513L}$, rJ.S$_{W513S}$, rJ.S$_{W513R}$) were selected, propagated, and titered as previously described (38). At least two independent isolates of each recombinant virus were plaque purified and analyzed.

Mice

Specific pathogen-free B6 and BALB/c mice were obtained from National Cancer Institute (Bethesda, MD). Suckling mice were infected intranasally with 2–4 $\times$ 10^4 PFU of recombinant JHMV at 10 days of age and nursed by JHMV-immune dams (39). After weaning, survivors of the acute infection were monitored for development of hindlimb paralysis out to 60 days p.i.. For experiments using epitope S510 variant viruses, half of each litter served as an internal control: one half of each litter was infected with variant virus, and the other half was infected with recombinant WT JHMV (rJ). All animal studies were approved by the University of Iowa Animal Care and Use Committee.

RNA sequence analysis

Total RNA was purified with TRIzol (Invitrogen) from the CNS of infected mice. The region encompassing epitope S510 was amplified by RT-PCR and PCR products sequenced directly as previously described (22).

One-step viral growth kinetics

Virus was inoculated onto confluent 17Cl-1 monolayers in a 12-well plate at a multiplicity of infection (MOI) of 1.0. Groups of cells were harvested at the indicated time points and total virus (cell-associated and cell-free) was titered as previously described (39).

In vitro and in vivo virus competition assays

For in vitro competition assays, equal PFU of rJ and rJ.S$_{W513G}$, rJ.S$_{W513L}$, rJ.S$_{W513S}$, or rJ.S$_{W513R}$ were combined (each at an MOI of 1) and inoculated onto confluent 17Cl-1 monolayers. Cell-free supernatants from infected cultures were sequentially passaged every 24 h for 4 days. At passages 2 and 4, total RNA was isolated from infected cells, and the relative representation of WT vs variant virus template was determined by RT-PCR followed by direct sequencing of PCR products. This assay can specifically detect a given species of template when that species comprises at least 20% of a heterogeneous pool (40). Two isolates of each rJ.S$_{W513}$ variant were assayed in triplicate, and the results from all six samples were pooled. For in vivo competition assays, equal PFU (2–4 $\times$ 10^4) of rJ and rJ.S$_{W513G}$, rJ.S$_{W513L}$, rJ.S$_{W513S}$, or rJ.S$_{W513R}$ were combined and mice were inoculated intranasally. Total RNA was harvested from the brains of mice 7 days p.i. and the relative representation of WT vs variant template was determined as described above.

Dendritic cell-based vaccination

LPS-matured dendritic cells (5 $\times$ 10^5) (DC) were prepared, coated with OVA or S510 peptides, and injected via tail vein into groups of 5-wk-old mice as previously described (41). Seven days following DC vaccination, mice were infected i.p. with 3 $\times$ 10^5 PFU rJ.S$_{W513G}$ or rJ.S$_{W513R}$. Seven days later, spleens were harvested from mice and the frequencies of epitope-specific CD8 T cells were determined by ex vivo peptide stimulation and intracellular cytokine staining as described below.

Intracellular cytokine staining and flow cytometry

Mononuclear cells were harvested from the brains of acutely ill mice 7 days p.i. and analyzed for expression of IFN-γ by an intracellular cytokine assay as previously described (42). Unless otherwise noted, peptides corresponding to the native S510 epitope or each S510 variant epitope were used at a final concentration of 1 μM. Cells were analyzed using a FACScan flow cytometer (BD Biosciences). Data sets were analyzed using FlowJo software (TreeStar). All Abs and reagents were purchased from BD Pharmingen.

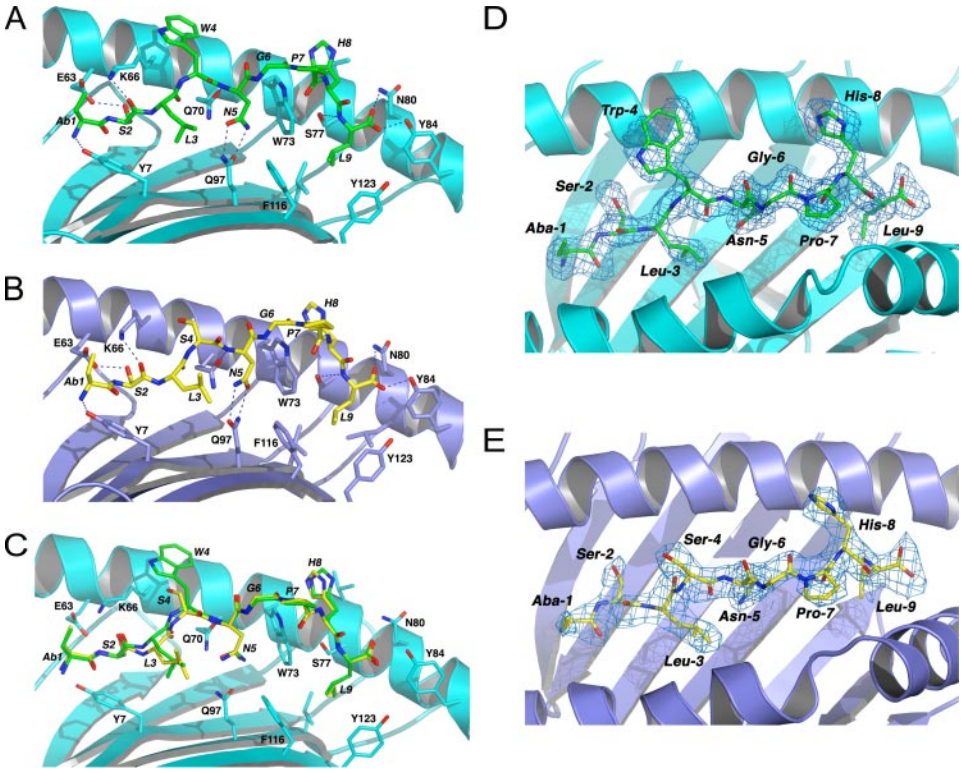

FIGURE 1. Refined structures of WT and W513S S510-Aba bound to H-2D^b. Cartoon representations of the Ag binding cleft in the refined H-2D^b structures, where the α2 helix (residues 124–180) has been removed to reveal the bound S510-Aba peptides. The peptide and selected residues of the H2-D^b H chain are shown in stick format. *A*, Refined model of H-2D^b in complex with epitope H-2D^b/$S_{510-518}$ (S510; CSLWNGPHL). The peptide is shown in green and the H-2D^b H chain in cyan. Key hydrogen bonding interactions are represented by dashed lines. Peptide residues are labeled in italics. *B*, Equivalent view in the structure of H-2D^b in complex with the W513S mutant of S510-Aba. H-2D^b is colored slate and the peptide is in yellow. *C*, Superposition of the WT and W513S peptides in their complex with H-2D^b. *D*, Cartoon representation of the H-2D^b Ag binding cleft as seen from above, with the WT S510-Aba peptide shown in stick format. *Overlay*: The unbiased F_o-F_c map density for the peptide contoured at 2 σ. *E*, Equivalent view of the W513S complex.

Peptide binding and stability assays

In some experiments, peptide binding was assessed using RMA-S cells as previously described (22). In other cases, the thermostability of recombinant MHC-peptide complexes were used to assess peptide binding using circular dichroism (CD). CD spectra were measured on a Jasco 810 spectropolarimeter using a thermostatically controlled cuvette at temperatures between 20 and 90°C as described in detail elsewhere (43, 44). Far-UV spectra from 195 to 250 nm were collected and averaged over 10 individual scans; 218 measurements for the thermal melting experiments were made at intervals of 0.1°C at a rate of 1°C/min. The midpoint of thermal denaturation (Tm) for each protein was calculated by taking the first derivative of the elipticity data and identifying the inflection point.

T cell functional avidity determination

Mononuclear cells were harvested from the brains of individual rJ-, rJ.S_{W513G}-, rJ.S_{W513L}-, rJ.S_{W513S}-, or rJ.S_{W513R}-infected mice 7 days p.i. and stimulated ex vivo in the presence of EL-4 cells pulsed with 10-fold dilutions of the relevant peptide. After 5.5 h, cells were stained for intracellular IFN-γ as described above. For each epitope-specific population, data were normalized to the frequency of Ag-specific CTL recorded at the highest titration of peptide (1 μM).

TCR Vβ-chain usage

Cells were harvested from the CNS of mice 7 days p.i. and stimulated ex vivo with S510 or $S510_{W513R}$ peptides. Cell aliquots were subsequently stained for CD8 (PE-Cy7-anti-CD8α) and each Vβ-chain (FITC-anti-Vβ2, 3, 4, 5.1/5.2, 6, 7, 8, 9, 10^b, 11, 12, 13, or 14) followed by intracellular staining for IFN-γ (PE-anti-IFN-γ). Data were collected using a BD LSR II instrument (BD Biosciences) at the University of Iowa Flow Cytometry Facility and are expressed as the frequency of Ag-specific CD8 T cells that express each Vβ-chain.

Results

Crystal structure of immunodominant JHMV CD8 T cell epitope H-2D^b/$S_{510-518}$

To evaluate the molecular nature of residues targeted for CTL escape during JHMV infection, we determined the crystal structure of the immunodominant JHMV CD8 T cell epitope H-2D^b/$S_{510-518}$ (S510; CSLWNGPHL). Initially, we observed that crystals of diffraction quality did not readily form due to oxidation of the N-terminal cysteine residue of S510 during in vitro refolding of the MHC-peptide complex. Substitution of this cysteine residue with L-α-aminobutyric acid (Aba), an isostereomer of cysteine, has previously been used to stabilize peptide epitopes (45). Aba-modified peptides are impervious to oxidative damage, cysteinylation, or dimerization, and in data not shown we demonstrated that Aba-modified S510 was equally stimulatory as native peptide when reacted with CNS-derived lymphocytes in IFN-γ intracellular staining assays. Furthermore, no additive effects were observed when mixtures of native and Aba-modified peptides were used to stimulate S510-specific CTL. Collectively, these results indicate that both peptides stimulate the same population of S510-specific CTL and validate the use of S510-Aba peptides for x-ray crystallographic analyses.

The structure of H-2D^b/S510-Aba consists of four heterodimers in the asymmetric unit, with each copy containing the S510-Aba peptide bound in the H chain's Ag-binding cleft (Fig. 1). In all four heterodimers the S-510 peptide, residues are highly ordered (Table III) and occupy virtually identical conformations (with root mean square deviation (rmsd) values of only 0.14 Å for all peptide atoms). Therefore, unless otherwise stated the structural features described below were observed in four copies.

The peptide adopts an extended conformation with a backbone kink at Pro^7. The side chains of Trp^4 and His^8 extend prominently out of the cleft and are predicted to dominate T cell recognition. MHC-anchoring interactions are made by Asn^5 and Leu^9 (Table IV). The peptide is anchored within the cleft primarily at positions 1, 2, 5, and 9. Aba^1 forms a hydrogen bond via its main chain with Tyr^7, Tyr^{159}, and Tyr^{171}, while its side chain is positioned within hydrogen bonding distance of Lys^{66}, suggesting a potential interaction for the original cysteine at that position. These interactions are consistent with a typical P1 amino acid complexed to H-2D^b, and they confirm the role of Aba as a potent peptidomimetic (Fig. 2).

Table III. *B factor analysis for the WT and W513S mutant S510-Aba peptides*[a]

Structure (Å^2)	Aba^1 (Cys^1)	Ser^2	Leu^3	Trp^4/Ser^4	Asn^5	Gly^6	Pro^7	His^8	Leu^9
H-2D^b/S510-Aba									
Overall B	20.9	19.6	21.8	20.1	14.0	14.8	14.2	12.3	14.3
Side chain B	21.8	19.6	23.7	21.1	13.0		15.4	11.5	13.9
H-2D^b/S510-W513S-Aba									
Overall B	13.7	13.4	13.9	14.1	15.0	15.3	15.2	15.4	15.4
Side chain B	13.7	13.0	13.9	13.3	15.1		15.1	15.5	15.4

[a] Presented are the average B factor values (in Å^2) for each peptide residue in the WT and W513S H2-D^b/S510-Aba structures, which were calculated using the CC4i implementation of BAVERAGE. The values given are for the entire residue (first and third rows), as well as for the side chain only (second and fourth rows).

Ser^2 hydrogen bonds with Glu^{63} and Lys^{66}, while Asn^5 is hydrogen bonded to Gln^{70} and Gln^{97}. The main chain of Leu^9 hydrogen bonds with Ser^{77}, Asn^{80}, Tyr^{84}, and Thr^{143}, while its side chain is buried within a hydrophobic pocket formed by Trp^{73}, Leu^{81}, Leu^{95}, Phe^{116}, Tyr^{123} and, Trp^{147} (Fig. 2).

Unlike the anchoring residues, positions 3, 4, 6, 7, and 8 are involved in fewer interactions with H-2D^b (Fig. 1*A*). Trp^4 is hydrogen bonded via its main chain carbonyl with His^{155}. Gly^6 and Pro^7 interact with Trp^{73} and Tyr^{156}, while His^8 interacts with Trp^{147} (Fig. 2).

Crystal structure of mutant W513SH-2D^b/S$_{510–518}$

We also determined the crystal structure of H-2D^b in complex with the W513S mutant of S510 (Fig. 1*B*), which contains a tryptophan to serine substitution at position 4 of the peptide in addition to having the cysteine at position 1 replaced by Aba. The structure of *W513S/H-2D^b/S$_{510–518}$* consists of two heterodimers in the asymmetric unit, with each copy containing the W513S S510-Aba peptide bound in the H chain's Ag-binding cleft. In both heterodimers the W513S peptide residues appear highly ordered (Fig. 1, *D* and *E*, Tables II and III) and occupy virtually identical conformations (rmsd values of only 0.06 Å for all peptide atoms). The peptide adopted the same structure as observed in the WT complex (rmsd for peptide C-alpha atoms between the two structures is 0.35 Å) and forms equivalent interactions with H-2D^b (Fig. 1*C*). The side chain of Ser^4 is oriented in the same way as the C-beta and C-gamma atoms of Trp^4 in the index peptide. The only notable deviations in structure are observed at positions 3 and 4, where the peptide backbone of the W513S mutant is shifted down into the cleft by ~0.7Å and is accompanied by a rearrangement in the side chain conformation of Leu^3. These minor differences may be due to the loss of steric clashes at position 4 in the W513S mutant and may account for the enhanced thermostability of the mutant complex.

CTL escape targets both TCR-accessible and anchor residues within the S510 epitope

Mutations at anchor residues are the simplest way for CTL escape variants to be generated, because they result in failure of the variant sequence to bind to the MHC. Consistent with this assumption, >25% of all CTL escape variants bear mutations at positions 2 and 5 (Table I). Interestingly, no mutations at Leu^9 were detected in mice, suggesting that mutation of anchor residues is not a global strategy for JHMV escape. Leu^3, another buried amino acid residue, is also a common target of immune escape, while the partially buried Cys^1 is never mutated in infected animals. Mutations are also commonly observed at Gly^6 and Pro^7, and such changes in these residues would most likely change the peptide's backbone conformation affecting TCR recognition. Mutations at the two most solvent accessible residues, Trp^4 and His^8, are expected to directly influence TCR recognition; however, only mutations at position 4 are detected. Moreover, the mutation at position 4 is restricted to Trp to Arg changes in >90% of persistently infected mice (Table I).

These data highlight the surprising diversity of CTL escape variants in this model and suggest multiple mechanisms of T cell escape. Even more surprising is the conservation of some variants, such as the propensity of Trp^4 to Arg^4 mutants. Single nucleotide changes in the Trp^4 could also result in mutations to Gly, Leu, Ser, and Cys. To begin to understand the basis of selectivity of CTL

Table IV. *Surface accessibility of the WT and W513S mutant S510-Aba peptides*[a]

	H-2D^b/S510-Aba			H-2D^b/S510-W513S-Aba		
Residue	Total Å^2 (%)	Main Chain	Side Chain	Total	Main Chain	Side Chain
Aba^1 (Cys^1)	1.7 (0.9)	0.0 (0.0)	1.7 (2.0)	2.8 (1.5)	0 (0.0)	2.8 (3.1)
Ser^2	2.7 (2.4)	0.7 (2.2)	2.0 (2.6)	5.4 (4.7)	1.2 (3.3)	4.2 (5.3)
Leu^3	4.1 (3.0)	2.0 (6.6)	2.1 (1.9)	5.1 (3.4)	1.7 (4.6)	3.4 (3.0)
Trp^4/Ser^4	128.0 (51.3)	2.7 (10.2)	125.3 (56.2)	49.2 (48.1)	4.2 (16.8)	45.0 (58.1)
Asn^5	15.8 (12.2)	15.8 (50.8)	0.0 (0.0)	20.7 (15.5)	20.7 (60)	0.0 (0.0)
Gly^6	28.8 (52.1)	28.8 (52.1)		28.9 (54.8)	28.9 (54.8)	
Pro^7	41.5 (31.6)	11.1 (35.5)	30.4 (30.4)	40.4 (31.1)	10.1 (33.4)	30.3 (30.4)
His^8	64.9 (36.5)	2.6 (9.0)	62.3 (41.9)	60.7 (34.3)	2.1 (6.6)	58.6 (40.3)
Leu^9	0.0 (0.0)	0.0 (0.0)	0.0 (0.0)	0.1 (0.0)	0 (0.0)	0.1 (0.1)
Trp^4 → Arg	141.8 (61.5)	4.8 (15.4)	137.0 (68.7)			
Trp^4 → Leu	91.4 (52.8)	2.9 (9.1)	88.5 (62.7)			
Trp^4 → Gly	32.1 (44.4)	32.1 (44.4)				

[a] Presented are the total, main chain, and side chain solvent-accessible surface of each peptide residue in the WT and W513S H2-D^b/S510-Aba structures, which were calculated using the CC4i implementation of AREAIMOL. Each cell displays the accessible area in Å^2, as well as a percentage of the surface available in the absence of H-2D^b (in parentheses). Also given are the accessible areas calculated after modeling an Arg, Leu, or Gly at position 4.

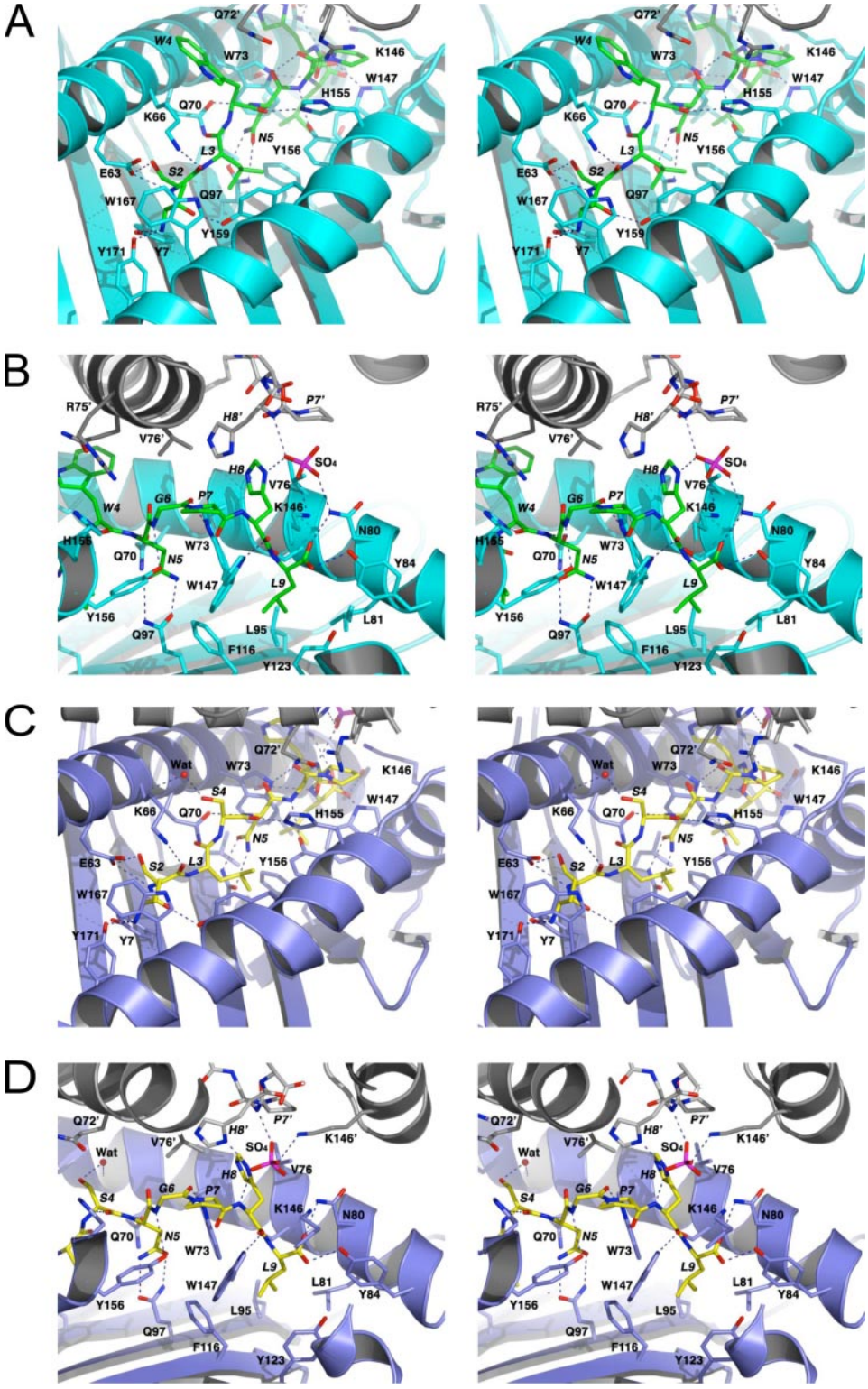

FIGURE 2. Images of the WT and W513S mutant S510-Aba peptides bound to H-2D^b. *A*, Cartoon representation of the refined model of H-2D^b/S510-Aba showing the Ag binding cleft from the peptide's N-terminus. All residues of S510-Aba (in green), as well as selected residues of the H-2D^b H chain (in cyan), are shown in stick format. Dashed lines represent key interactions between S510-Aba and H-2D^b. Also shown are residues of a crystallographically related molecule (in gray) involved in crystal contacts with the Ag binding cleft, as well as an ordered sulfate ion observed at the interface between symmetry-related peptide chains. Peptide residues are labeled in italics and residues from the symmetry-related molecule are labeled with an inverted comma. *B*, The H-2D^b/S510-Aba Ag binding cleft viewed from the peptide's C-terminal. A section of the α2 helix of the H chain has been removed to reveal the bound peptide. *C* and *D*, Equivalencies to *A* and *B* for the W513S H-2D^b/$S_{510-518}$ structure. In these images the H-2D^b H chain is drawn in slate and the W513S mutant S510-Aba peptide is shown in yellow.

escape at position 4, we compared the serological stability and thermostability of the D^b/S510 and four variant complexes (Arg^4, Gly^4, Leu^4, and Ser^4, also referred to as W513R/G/L/S) using the TAP1/2-deficient RMA-S cell line (46) and CD analyses. We found no difference in the ability of the variant peptides to bind H-2D^b in epitope stabilization assays (Fig. 3*A*). However, individual substitutions at Trp^4 altered the thermostability of epitope S510/H-2D^b complexes. The Gly*4* variant peptide was least able to stabilize the complex, relative to the other variant epitopes. This is consistent with a stabilizing role of van der Waals interactions between the indole side chain of the Trp residue and H-2D^b. In contrast, the Ser^4 variant epitope enhanced the stability of H-2D^b complexes (Fig. 3*B*). Taken together, these results support the structural studies that indicate that position 4 of the S510 epitope is primarily involved in TCR recognition. However, some substitutions, such as Gly^4 or Ser^4, can also subtly influence the stability of the H-2D^b/epitope complex.

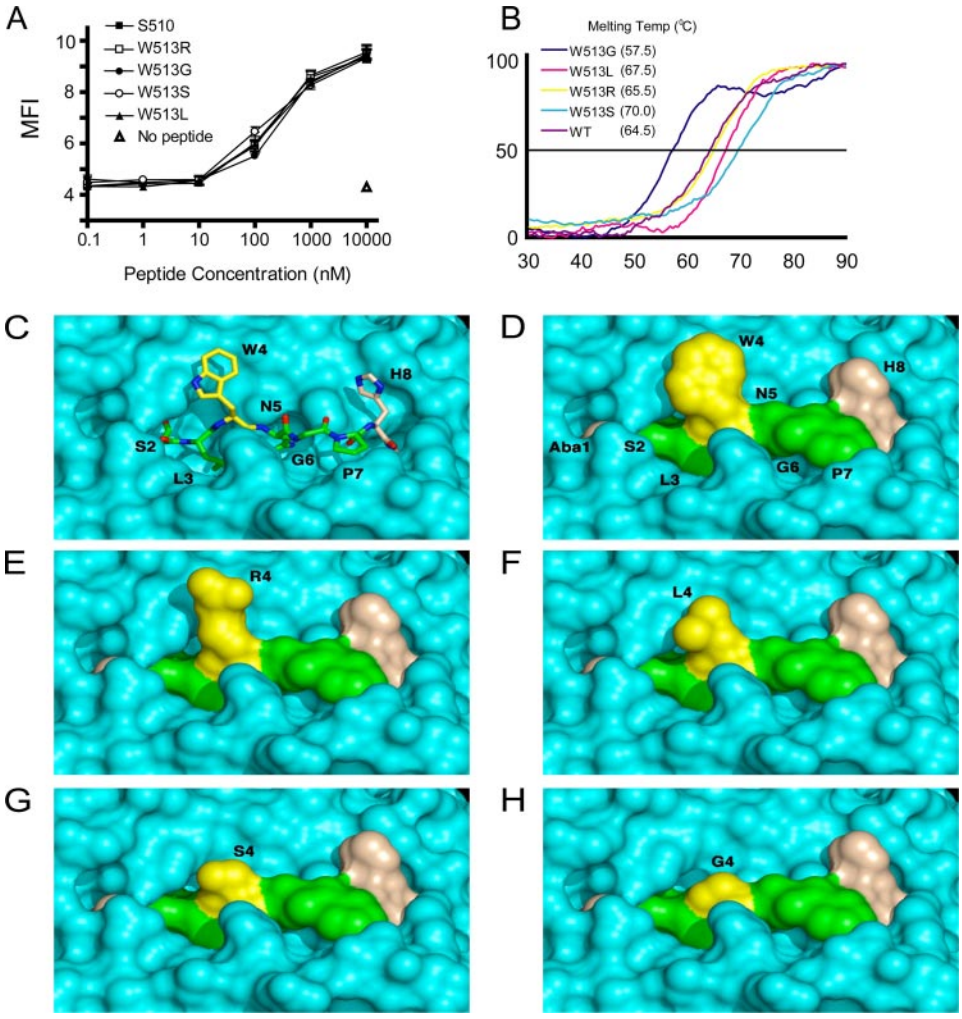

FIGURE 3. H-2D^b binding and surface accessibility of the S510-Aba peptide. *A*, RMA-S cells were incubated in the presence of the indicated concentrations of peptides corresponding to the native S510 epitope or each variant epitope and analyzed for surface H-2D^b as described in *Materials and Methods*. Data are means ± SEM for four independent experiments. *B*, CD analysis of native epitope S510 and each variant epitope complexed with H-2D^b. CD spectra were measured as described in *Materials and Methods*. *C*, Surface representation of H-2D^b (cyan), showing the bound S510-Aba peptide in stick format. Those peptide residues where mutations are never observed have carbon atoms drawn in wheat color. Trp^4 is drawn with yellow carbons, while the other residues for which mutations have been detected have green carbons. *D*, Identical view of the H-2D^b/S510-Aba complex, but with a surface representation of the peptide. The color scheme use in *C* has been maintained. *E–H*, To gauge the effect of mutating Trp4 to either an Arg, Leu, Ser, or Gly, each of these residues was modeled at position 4 using Coot: (*E*) arginine, (*F*) leucine, (*G*) serine, and (*H*) glycine.

Next, we used the WT and W513S mutant H-2D^b/S510 complexes as templates for modeling how the mutations at position 4 could influence binding to S510-specific TCR. Of the four mutants, only the arginine substitution cannot be accommodated within the space occupied by the tryptophan's indole ring, due to unfavorable contacts between its guanadinium group and H-2D^b, which results in an altered side chain orientation (Fig. 3, *C–H*). Consequently, the side chain in the Arg^4 variant would be expected to extend out of the Ag binding cleft and interfere with WT-specific CTL recognition, while the Leu and Gly mutations could be accommodated with minimal structural perturbations, as was the case for the Ser^4 variant peptide complex. The difference in polarity and size between these residues and the native Trp, however, is substantial and is predicted to significantly affect TCR recognition.

rJ and Trp^4 variant viruses are equally fit in tissue culture cells and in mice with acute encephalitis

The structural data highlight why mutation at Trp^4 results in evasion of the epitope S510-specific CD8 T response, but they do not explain the lack of outgrowth of Gly^4, Leu^4, and Ser^4 variant viruses in persistently infected mice. To directly test whether functional constraints on virus fitness explain these results, we generated a series of isogenic recombinant viruses encoding Gly^4, Leu^4, and Ser^4 substitutions (herein referred to as rJ.S$_{W513G}$, rJ.S$_{W513L}$, and rJ.S$_{W513S}$, respectively). Recombinant WT virus (rJ) and virus encoding the Arg^4 substitution (rJ.S$_{W513R}$) were also generated. We found no differences among the viruses in analyses of one-step growth kinetics in 17Cl-1 cells (Fig. 4*A*). Furthermore, there were no marked differences following in vitro competition assays in which relative recovery of rJ vs each variant was assessed by RT-PCR and sequencing (Fig. 4*B*). In general, rJ outgrew variant viruses in 17Cl-1 cells, although mutated virus was still detected after four passages in 50% or more of cultures (Fig. 4*C*). In vitro analyses may not reflect the relative replicative capacity of viruses within the intact animal. However, all of the variant viruses grew as least as well as rJ in B6 mice and in BALB/c (H-2^d) mice, which do not recognize epitope S510 and therefore do not exert immune selection on this region of the virus (Fig. 4*D*).

Viruses encoding W513R/S but not W513G/L cause enhanced disease in Ab-protected infected mice

We previously showed that when Ab-protected, suckling mice are infected with naturally occurring CTL escape viruses, the mice exhibit increased morbidity and mortality, relative to infection with WT JHMV (23). Thus, as a measure of in vivo virus fitness, we infected maternal Ab-protected, suckling mice with WT or variant S510 recombinant viruses (Fig. 4*E*). As expected, ~80% of mice infected with rJ survived the acute infection. By comparison, rJ.S$_{W513S}$ and rJ.S$_{W513R}$ behaved as expected for true CTL escape variants, with only 20% of infected mice surviving the acute infection (death before 14 days

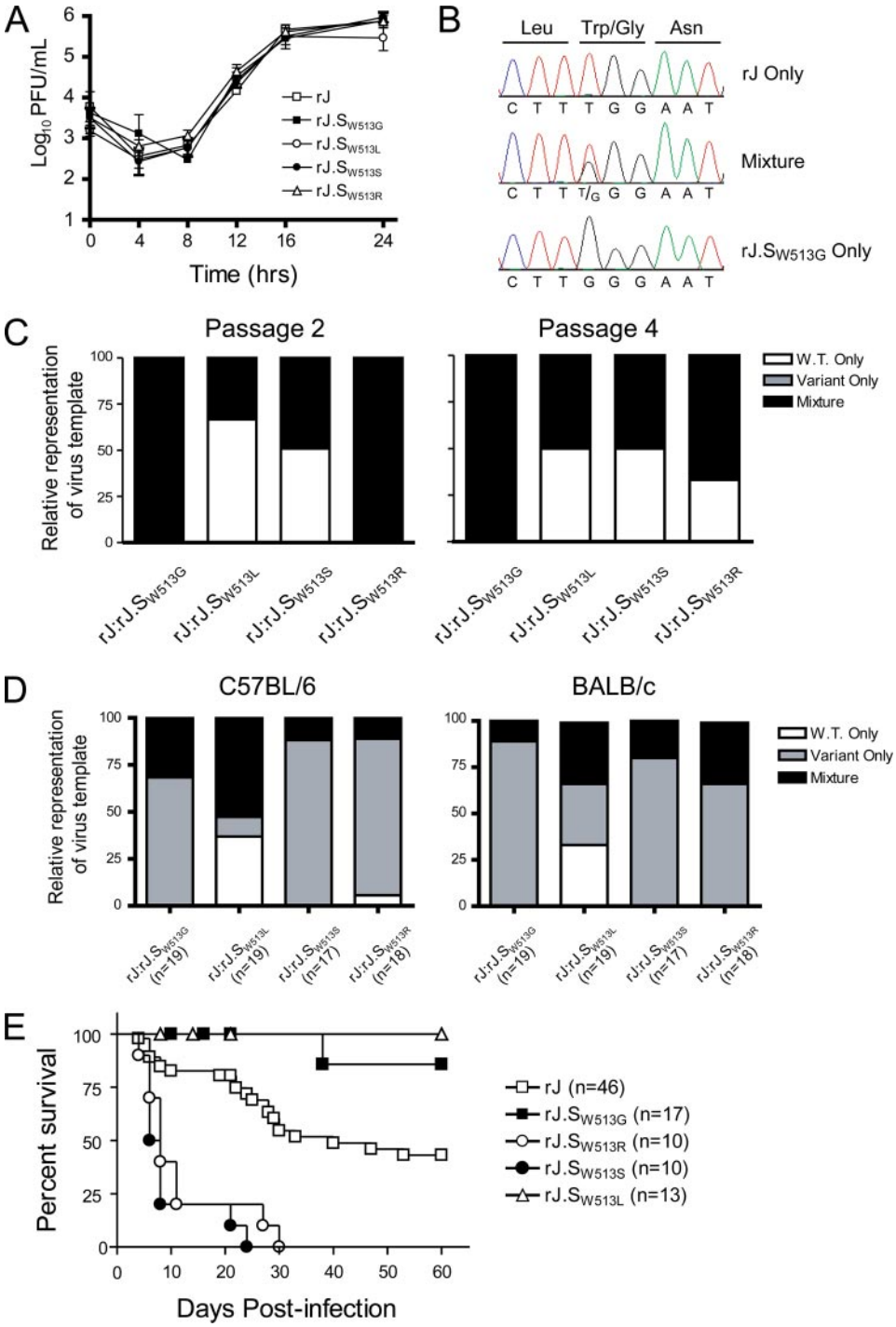

FIGURE 4. In vitro and in vivo growth comparisons of rJ and rJ.S_{W513} variant viruses. *A*, 17Cl-1 cells were infected with rJ and rJ.S_{W513} variant viruses at an MOI of 1.0. Cells and supernatants were harvested at the indicated times, and titers were measured by plaque assay on Hela-MHVR cells as described in *Materials and Methods*. Data are means ± SEM for three independent experiments. *B*, Representative sequencing chromatograms from RT-PCR analyses of brain RNA samples in which only rJ (*top*), a mixture of rJ and rJ.S_{W513G} (*middle*), or only rJ.S_{W513G} (*bottom*) virus templates were detected. *C*, 17Cl-1 cells were infected with equal PFU of rJ and each variant (MOI of 1) and propagated for four passages. Total RNA was harvested from infected wells at passages 2 (*left panel*) and 4 (*right panel*) and relative representation of rJ or variant was determined as described in *Materials and Methods*. Data for passages 2 and 4 are pooled results obtained by analyzing 6 wells for each virus mixture. *D*, B6 mice (*left panel*) and BALB/c (*right panel*) mice were infected with virus mixtures consisting of equal PFU of rJ and each variant. Seven days later total RNA was harvested from the brains of infected mice and relative representation of virus template was determined via RT-PCR and direct sequencing of PCR products as described in *Materials and Methods*. Numbers in parentheses indicate the number of mice examined for each group. *E*, Survival analysis of maternal Ab-protected suckling mice infected with rJ or rJ.S_{W513} variant viruses. Mice were scored as deceased after developing clinical signs of hindlimb paralysis/paresis (day of tissue harvest).

p.i.). Less expected were the results for mice infected with rJ.S_{W513G} and rJ.S_{W513L} viruses: we found substantially less morbidity and mortality during infection with either virus when compared with rJ-infected mice. These results are remarkable given that both rJ.S_{W513G} and rJ.S_{W513L} viruses cause lethal encephalitis in mice not protected by maternal Abs, and they compete with rJ in acutely infected adult animals. This inability to cause encephalitis suggests that the Leu^4 and Gly^4 mutations would not outgrow rJ even if the mutations arose in persistently infected mice. As described below, this may reflect differences in cellular tropism or inflammatory milieu in persistently as opposed to acutely infected mice. Subsequently, we focused on the Ser^4 mutation, which should be (but is not) selected in persistently infected mice.

Recombinant viruses bearing Arg^4, but not Ser^4, substitutions prime CTL responses

Another possibility is that de novo CTL responses develop to the Ser^4, but not Arg^4, variants, thereby minimizing the likelihood that this variant would be selected in vivo. First, we demonstrated that CNS-derived WT S510-specific CD8 T cells do not recognize either variant epitope in direct ex vivo intracellular IFN-γ staining assays (Fig. 5*A*, Table V), confirming results obtained with splenic cells (29). Next, to determine whether either variant elicited a novel CTL response, we assayed CNS-derived lymphocytes from variant virus-infected mice for epitope-specific CD8 T cell responses. We found that mice mounted a low-level CD8 T cell response to the Arg^4 epitope, but no response to the Ser^4 epitope

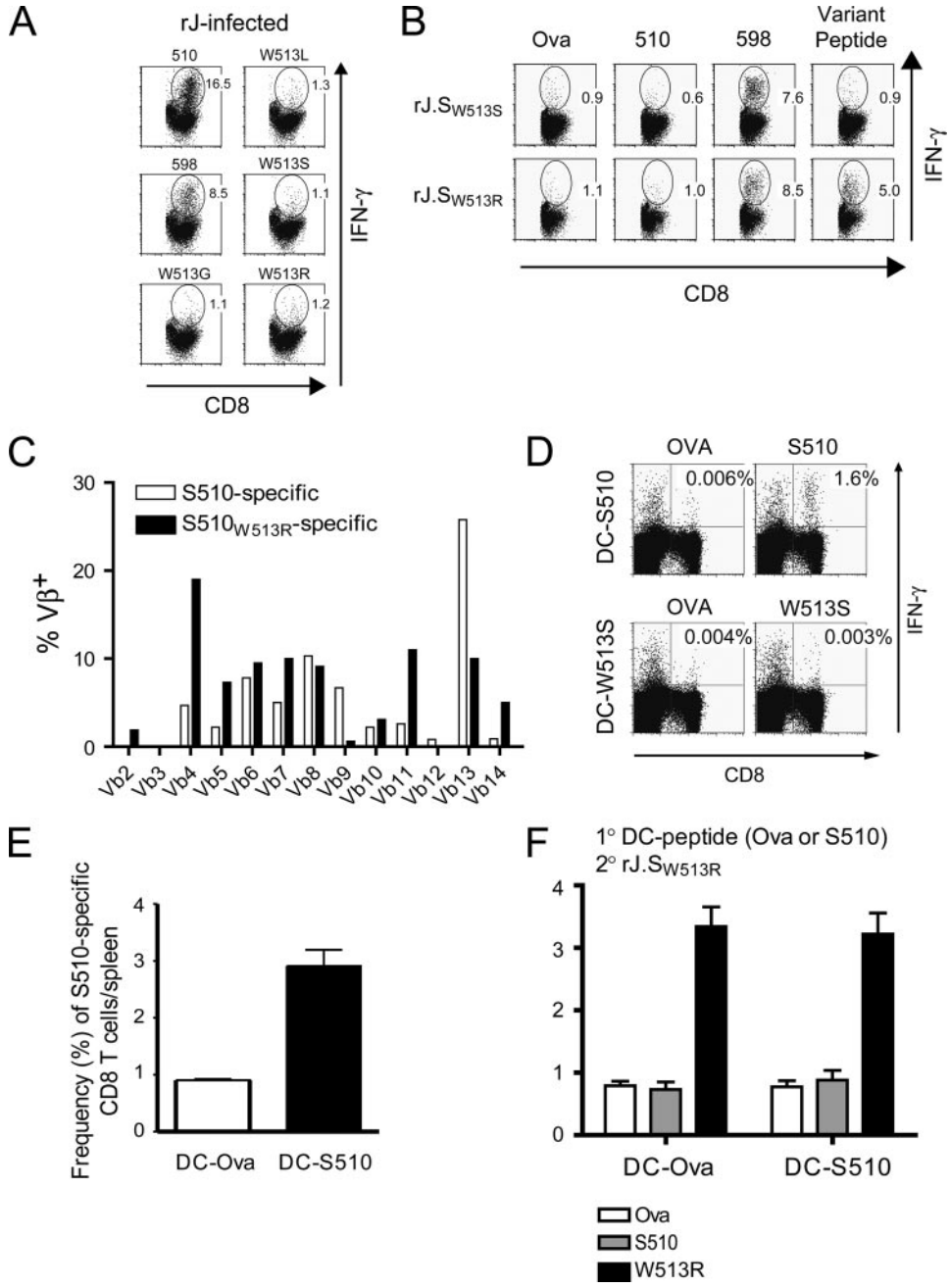

FIGURE 5. De novo recognition of variant S510 epitopes in variant virus-infected B6 mice. *A*, Dot plots demonstrating ex vivo detection of epitope S510- and S598-specific CD8 T cells from the brain of a representative rJ-infected mouse. Approximately 1% of cells produced IFN-γ when stimulated with peptides corresponding to any of the variant epitopes or an irrelevant peptide (OVA, not shown). *B*, Dot plots demonstrating recognition of variant epitopes by CD8 T cells isolated from the brains of mice infected with rJ.S_{W513S} or rJ.S_{W513R} viruses. Seven days p.i., CNS-derived mononuclear cells were stimulated ex vivo with peptides corresponding to irrelevant control (OVA), native S510, subdominant S598, or matching variant epitopes. Numbers in *A* and *B* represent percentages of IFN-γ^+CD8^+ cells for each virus-infected mouse. *C*, TCR Vβ-chain usage between S510- and $S510_{W513R}$-specific CD8 T cells. Total mononuclear cells were harvested from mice infected with rJ or rJ.S_{W513R} and stimulated ex vivo with the peptides corresponding to native S510 and $S510_{W513R}$ epitopes, respectively. Following stimulation, aliquots of cells were surface stained for CD8 and the indicated Vβ-chain followed by intracellular cytokine staining for IFN-γ. Data represent the fraction of IFN-γ^+CD8^+ T cells expressing each Vβ-chain and are derived from cells pooled from 2–3 individual mice. *D*, Representative dot plots demonstrating detection of epitope-specific CD8 T cells in the spleens of mice 7 days after vaccination with S510- or $S510_{W513S}$-coated DCs. Data shown are representative of four independent experiments. *E*, Frequency of S510-specific CD8 T cells in the spleens of mice 7 days after vaccination with OVA peptide- or S510 peptide-coated DCs. Data are means ± SEM for 3 individual mice. *F*, Frequency of $S510_{W513R}$-specific CD8 T cells in the spleens of mice after DC-peptide priming followed by peripheral infection with rJ.S_{W513R} virus. Data are means ± SEM for 3 individual mice and are representative of three independent experiments.

(Fig. 5*B* and Table V). Based on the modeled structures, the Arg^4 variant is predicted to elicit a TCR profile different from that elicited by the WT epitope; consistent with this prediction, S510- and $S510_{W513R}$-specific CTL exhibit different TCR Vβ-chain profiles (Fig. 5*C*) with the emergence of Vβ4 and $V\beta11^+$ T cell populations and retraction of the $V\beta13^+$ population.

The lack of priming to Ser^4 could reflect differences in Ag processing and presentation of this variant epitope or a hole in

Table V. *Frequency of total and epitope-specific CD8 T cells in the CNS of recombinant WT MHV and S510 variant-infected mice*[a]

Virus	No. MNC/CNS ($\times 10^6$)	Frequency (%) CD8 T Cells/CNS	Frequency (%) Native S510-Specific[b]	Frequency (%) S510 Variant-Specific[c]
rJ ($n = 4$)	1.83 ± 0.43	13.4 ± 1.4	15.3 ± 1.59	1.55 ± 0.06[d]
rJ.S$_{W513S}$ ($n = 8$)	1.72 ± 0.22	12.6 ± 3.2	1.04 ± 0.14	1.07 ± 0.16
rJ.S$_{W513R}$ ($n = 7$)	1.65 ± 0.34	14.5 ± 2.5	1.24 ± 0.36	4.17 ± 0.94

[a] Values are expressed as means ± SEM.
[b] As measured by direct ex vivo intracellular cytokine staining assay using the native peptide S510 epitope.
[c] As measured after ex vivo stimulation using the corresponding S510 variant epitope peptide.
[d] Data for rJ are pooled results using each of the S510 variant epitope peptides in the ex vivo stimulation.

the TCR repertoire. To address the latter possibility, we evaluated the ability of the Ser^4 epitope to prime CTL responses using peptide-pulsed DC-based vaccination. We found that the Ser^4 epitope failed to prime a CTL response, while native S510-pulsed DCs primed a robust response (Fig. 5*D*). Therefore, the lack of priming to Ser^4 likely reflects a hole in the TCR repertoire or tolerance to this epitope. These results further suggest that the Ser^4 variant should be selected in persistently infected mice.

The response to epitope Arg^4 was unexpected because virus expressing this variant epitope is recovered in vivo and is highly virulent. One possible explanation was that in mice persistently infected with rJ, the phenomenon of original antigenic sin occurred (expansion of native epitope-specific CTL, rather than priming a de novo variant-specific CTL response (47)). To explore this possibility, we used a combination of DC-S510 peptide priming followed by peripheral infection with rJ.S$_{W513R}$. However, as shown in Fig. 5, *E* and *F*, we found that these mice mount splenic CD8 T cell responses of similar magnitude to the Arg^4 variant epitope, regardless of whether they were vaccinated with DC-S510 or DC-OVA (an irrelevant epitope), and they do not mount a secondary response to the WT epitope.

To further assess the biological significance of this modest S510$_{W513R}$-specific CD8 T cell response, we examined the functional avidity of these cells. As shown in Fig. 6, the relative functional avidity of CNS-derived cells responding to the native and the variant epitopes was not different. A low functional avidity may have explained why the response does not prevent the outgrowth of variant viruses expressing the Arg^4 epitope; however, this does not appear to be the case for this escape variant.

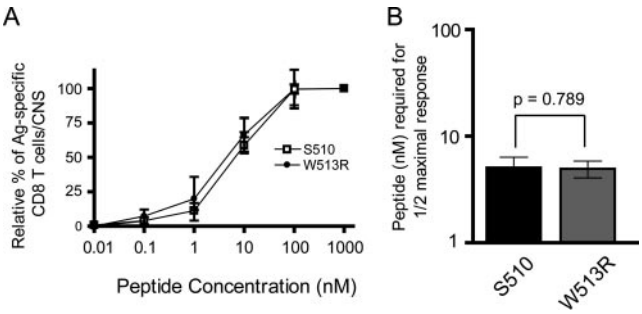

FIGURE 6. Functional avidity of S510$_{W513R}$-specific CD8 T cells. *A*, Mononuclear cells were harvested from mice infected with rJ or rJ.S$_{W513R}$ at 7 days p.i. and stimulated ex vivo in the presence of 10-fold dilutions of the relevant peptides. The frequency of epitope-specific CD8 T cells per brain was determined as described in *Materials and Methods*. For each group, data are normalized to the frequency of epitope-specific CD8 T cells observed using 1 μM of peptide. *B*, Data from *A* plotted as a function of the amount of peptide required to elicit the one-half maximal response. Data shown are means ± SEM for 4–5 individual mice and are representative of three independent experiments.

Discussion

Herein, we combine structural studies of the H-2D^b/S510 epitope and a nonselected variant W513S S510 epitope with biological studies of viruses expressing variant epitopes to begin to understand selectivity in CTL escape development. While the structures of CTL variants of a single epitope (lymphocytic choriomeningitis virus (LCMV) gp33) have been solved (48), our study is the first to combine structural analyses with biological assays using recombinant viruses expressing variant epitopes. Our results show that selection is more complicated than previously postulated because a mutation, W513S, that results in CTL evasion without impairing virus replication is not selected in infected mice. Previous reports have concluded that some CTL escape variants are not selected because they compromise virus fitness. Moreover, many of those that do become selected are postulated to negatively affect virus fitness, as evidenced by rapid reversion to WT sequence when transmitted to hosts that lack the appropriate restriction element, or the requirement for co-selection of compensatory mutations that restore virus fitness (8, 49, 50). In a few cases, deleterious effects on virus fitness have been demonstrated directly in in vitro assays, using tissue culture cells or virus replicons (11, 50, 51). Consequently, a conclusion from these studies is that only a few mutations are selected because, despite their ability to evade CTL recognition, the vast majority negatively impact virus fitness. However, our results indicate that epitope diversification is also limited by features other than virus fitness, as discussed below.

The epitope S510 mutation at position 4 that is selected in vivo, Trp to Arg, alters the topology of the D^b/S510 complex and likely directly diminishes or abrogates binding by the TCR. Other studies showed that single amino acid changes that result in altered topology of the epitope/MHC complexes can significantly skew the TCR repertoire. For example, an Arg to Ala mutation at position 7 of the influenza A-specific PA224 epitope, which removes the most prominent feature of the complex (52), still induces a CD8 T cell response, but it is much less diverse compared with the response to the native epitope. Similarly, we observed that the Trp to Arg single amino acid change in epitope S510 significantly altered the TCR repertoire distribution of responding CTL based on Vβ usage (Fig. 5C). The importance of the Trp^4 determinant is also illustrated by the complete abrogation of the response by other mutations, including Leu, Gly, and Ser. This focus on a single amino acid residue is especially notable because the S510-specific response is highly diverse, consisting of ~1000–2000 different TCR clonotypes (53, 54); thus, although the response is highly diverse, it is functionally monospecific.

We expected that the lack of recovery of Gly^4, Leu^4, and Ser^4 variants would be explained by significant deleterious effects on virus fitness, as has been described for certain mutations in CTL epitopes derived from HIV, SIV, or HCV (11, 50, 51). However, our results demonstrate that effects of mutations on fitness may be

very subtle and appear only under certain conditions. For example, while there were no gross effects on fitness in either acutely infected adult mice or tissue culture cells (Fig. 4, *A*, *C*, and *D*), both the Gly^4 and Leu^4 substitutions result in a nearly complete loss of virulence in Ab-protected suckling mice (Fig. 4*E*). One difference between mice with acute lethal encephalitis and maternal Ab-protected mice is that different types of CNS cells are predominantly infected in each scenario. In mice with acute encephalitis, neurons are preferentially infected, whereas glial cells (oligodendrocytes, microglia, and astrocytes) are infected in persistently infected mice, including those protected by maternal Ab (39, 55–58). Single amino acid changes in the JHMV S glycoprotein have been shown to change tropism from glia to neurons in previous studies (59, 60); one possibility is that $rJ.S_{W513G}$ and $r.J.S_{W513L}$ exhibit diminished growth in one or more type of glial cell in vivo when compared with $rJ.S_{W513S}$ and $r.J.S_{W513R}$.

In addition to virus tropism, the inflammatory milieu of the acute vs persistently infected CNS may differ with perhaps important and direct effects on local T cell responses and the resultant selective pressure exerted by CTL. Inflammation, MHC class I expression, and CTL effector function wane dramatically during persistent JHMV infection (61, 62). Similar effects on CTL have been observed in mice persistently infected with LCMV and humans chronically infected with HIV (63–66) and they correlate with PD-1 expression on dysfunctional CTL (67, 68). Thus, in maternal Ab-protected, persistently infected mice, the role of S510-specific CD8 T cells in driving diversification may be less potent than in acutely infected mice. If viruses, such as $rJ.S_{W513G}$ and $rJ.S_{W513L}$, are subtly less fit in the persistently infected animal, a diminished CTL response would result in less immune pressure and perhaps in the lack of continued outgrowth of these viruses, even though they express mutations predicted to abrogate the CTL response.

Although these results provide a partial explanation for why some mutations (Leu^4 and Gly^4) that abrogate the S510-specific response are not selected in mice, the lack of selection of variant viruses encoding W513S mutations is puzzling. This mutation does not affect virus viability, and $rJ.S_{W513S}$ behaves like a CTL escape virus, causing disease severity equivalent to that of $rJ.S_{W513R}$ when inoculated into Ab-protected suckling mice (Fig. 4*E*). Furthermore, there is no recognition of this epitope in B6 mice (Fig. 5, *B* and *D*), suggesting a hole in the TCR repertoire. In support of this possibility, we have identified a nonamer in murine ADAM23 that is predicted to bind $H\text{-}2D^b$ (CSLSNGAHC) and could potentially induce deletion of epitope $S510_{W513S}$-specific CD8 T cells during thymic selection. We also considered the possibility that the lack of outgrowth of the Ser^4 variant might be explained by functional constraints related to codon usage or transition (vs transversion) mutation bias, as has been described for hepatitis G virus (HGV) (69). Transition mutations are favored by a factor of 10^4 in HGV-infected cells, but both a transition (UGG to CGG) and a transversion (UGG to AGG) result in the W513R mutation and both occur with the same frequency.

Our results showing enhanced virulence of viruses encoding Arg^4 or Ser^4 substitutions demonstrate a critical protective role for S510-specific CTL in Ab-protected mice. Although worsened disease is likely related to enhanced virus replication, the effect may also involve immunopathologic mechanisms, with the anti-JHMV CD4 T cell response largely responsible for clinical disease (38, 42). Thus, it is possible that enhanced disease occurs in mice infected with CTL escape virus, because increased virus replication elicits a compensatory antiviral CD4 T cell response, with immunopathological consequences.

Collectively, our results suggest that, at least for some variant epitopes, the forces that influence the selection of CTL escape variant viruses are complex and extend beyond the postulates of virus fitness and de novo CTL recognition. Thus, additional understanding of the immune response during persistent viral infection may be key to understanding the mechanisms of CTL escape. For example, subtle changes in cell tropism and/or replicative capacity during persistence may shape the unique subset of CTL escape mutations that are selected. The monospecific nature of antiviral T cells responding to the immunodominant S510 epitope results in JHMV viral escape, suggesting that the avoidance of such focused responses by targeted vaccination programs is warranted.

Acknowledgments

We thank the staff at the Advanced Photon Source and the Australian Synchrotron for assistance with data collection and John T. Harty for critical reading of the manuscript.

Disclosures

The authors have no financial conflicts of interest.

References

1. Yewdell, J. W. 2006. Confronting complexity: real-world immunodominance in antiviral $CD8^+$ T cell responses. *Immunity* 25: 533–543.
2. Oxenius, A., D. A. Price, A. Trkola, C. Edwards, E. Gostick, H. T. Zhang, P. J. Easterbrook, T. Tun, A. Johnson, A. Waters, et al. 2004. Loss of viral control in early HIV-1 infection is temporally associated with sequential escape from $CD8^+$ T cell responses and decrease in HIV-1-specific $CD4^+$ and $CD8^+$ T cell frequencies. *J. Infect. Dis.* 190: 713–721.
3. Perlman, S., and L. Pewe. 1998. Role of CTL mutants in demyelination induced by mouse hepatitis virus, strain JHM. *Adv. Exp. Med. Biol.* 440: 515–519.
4. Goulder, P. J., and D. I. Watkins. 2004. HIV and SIV CTL escape: implications for vaccine design. *Nat. Rev. Immunol.* 4: 630–640.
5. McMichael, A. J., and R. E. Phillips. 1997. Escape of human immunodeficiency virus from immune control. *Annu. Rev. Immunol.* 15: 271–296.
6. Bowen, D. G., and C. M. Walker. 2005. Mutational escape from $CD8^+$ T cell immunity: HCV evolution, from chimpanzees to man. *J. Exp. Med.* 201: 1709–1714.
7. Berkhoff, E. G., E. de Wit, M. M. Geelhoed-Mieras, A. C. Boon, J. Symons, R. A. Fouchier, A. D. Osterhaus, and G. F. Rimmelzwaan. 2005. Functional constraints of influenza A virus epitopes limit escape from cytotoxic T lymphocytes. *J. Virol.* 79: 11239–11246.
8. Friedrich, T. C., E. J. Dodds, L. J. Yant, L. Vojnov, R. Rudersdorf, C. Cullen, D. T. Evans, R. C. Desrosiers, B. R. Mothe, J. Sidney, et al. 2004. Reversion of CTL escape-variant immunodeficiency viruses in vivo. *Nat. Med.* 10: 275–281.
9. Jones, N. A., X. Wei, D. R. Flower, M. Wong, F. Michor, M. S. Saag, B. H. Hahn, M. A. Nowak, G. M. Shaw, and P. Borrow. 2004. Determinants of human immunodeficiency virus type 1 escape from the primary $CD8^+$ cytotoxic T lymphocyte response. *J. Exp. Med.* 200: 1243–1256.
10. Peyerl, F. W., D. H. Barouch, W. W. Yeh, H. S. Bazick, J. Kunstman, K. J. Kunstman, S. M. Wolinsky, and N. L. Letvin. 2003. Simian-human immunodeficiency virus escape from cytotoxic T-lymphocyte recognition at a structurally constrained epitope. *J. Virol.* 77: 12572–12578.
11. Soderholm, J., G. Ahlen, A. Kaul, L. Frelin, M. Alheim, C. Barnfield, P. Liljestrom, O. Weiland, D. R. Milich, R. Bartenschlager, and M. Sallberg. 2006. Relation between viral fitness and immune escape within the hepatitis C virus protease. *Gut* 55: 266–274.
12. Allen, T. M., X. G. Yu, E. T. Kalife, L. L. Reyor, M. Lichterfeld, M. John, M. Cheng, R. L. Allgaier, S. Mui, N. Frahm, et al. 2005. De novo generation of escape variant-specific $CD8^+$ T-cell responses following cytotoxic T-lymphocyte escape in chronic human immunodeficiency virus type 1 infection. *J. Virol.* 79: 12952–12960.
13. Bailey, J. R., T. M. Williams, R. F. Siliciano, and J. N. Blankson. 2006. Maintenance of viral suppression in HIV-1-infected $HLA\text{-}B*57^+$ elite suppressors despite CTL escape mutations. *J. Exp. Med.* 203: 1357–1369.
14. Allen, T. M., M. Altfeld, S. C. Geer, E. T. Kalife, C. Moore, M. O'Sullivan, K., I. Desouza, M. E. Feeney, R. L. Eldridge, E. L. Maier, et al. 2005. Selective escape from $CD8^+$ T-cell responses represents a major driving force of human immunodeficiency virus type 1 (HIV-1) sequence diversity and reveals constraints on HIV-1 evolution. *J. Virol.* 79: 13239–13249.
15. Turnbull, E. L., A. R. Lopes, N. A. Jones, D. Cornforth, P. Newton, D. Aldam, P. Pellegrino, J. Turner, I. Williams, C. M. Wilson, et al. 2006. HIV-1 epitope-specific $CD8^+$ T cell responses strongly associated with delayed disease progression cross-recognize epitope variants efficiently. *J. Immunol.* 176: 6130–6146.
16. Altfeld, M., M. M. Addo, E. S. Rosenberg, F. M. Hecht, P. K. Lee, M. Vogel, X. G. Yu, R. Draenert, M. N. Johnston, D. Strick, et al. 2003. Influence of HLA-B57 on clinical presentation and viral control during acute HIV-1 infection. *AIDS* 17: 2581–2591.
17. Migueles, S. A., M. S. Sabbaghian, W. L. Shupert, M. P. Bettinotti, F. M. Marincola, L. Martino, C. W. Hallahan, S. M. Selig, D. Schwartz, J. Sullivan, and M. Connors. 2000. HLA B*5701 is highly associated with restriction of virus replication in a subgroup of HIV-infected long term nonprogressors. *Proc. Natl. Acad. Sci. USA* 97: 2709–2714.

18. Kaslow, R. A., M. Carrington, R. Apple, L. Park, A. Munoz, A. J. Saah, J. J. Goedert, C. Winkler, S. J. O'Brien, C. Rinaldo, et al. 1996. Influence of combinations of human major histocompatibility complex genes on the course of HIV-1 infection. *Nat. Med.* 2: 405–411.
19. Muhl, T., M. Krawczak, P. Ten Haaft, G. Hunsmann, and U. Sauermann. 2002. MHC class I alleles influence set-point viral load and survival time in simian immunodeficiency virus-infected rhesus monkeys. *J. Immunol.* 169: 3438–3446.
20. O'Connor, D. H., T. M. Allen, T. U. Vogel, P. Jing, I. P. DeSouza, E. Dodds, E. J. Dunphy, C. Melsaether, B. Mothe, H. Yamamoto, et al. 2002. Acute phase cytotoxic T lymphocyte escape is a hallmark of simian immunodeficiency virus infection. *Nat. Med.* 8: 493–499.
21. O'Connor, D., T. Friedrich, A. Hughes, T. M. Allen, and D. Watkins. 2001. Understanding cytotoxic T-lymphocyte escape during simian immunodeficiency virus infection. *Immunol. Rev.* 183: 115–126.
22. Pewe, L., G. F. Wu, E. M. Barnett, R. F. Castro, and S. Perlman. 1996. Cytotoxic T cell-resistant variants are selected in a virus-induced demyelinating disease. *Immunity* 5: 253–262.
23. Pewe, L., S. Xue, and S. Perlman. 1998. Infection with cytotoxic T-lymphocyte escape mutants results in increased mortality and growth retardation in mice infected with a neurotropic coronavirus. *J. Virol.* 72: 5912–5918.
24. Ontiveros, E., L. Kuo, P. S. Masters, and S. Perlman. 2001. Inactivation of expression of gene 4 of mouse hepatitis virus strain JHM does not affect virulence in the murine CNS. *Virology* 289: 230–238.
25. Barouch, D. H., J. Kunstman, M. J. Kuroda, J. E. Schmitz, S. Santra, F. W. Peyerl, G. R. Krivulka, K. Beaudry, M. A. Lifton, D. A. Gorgone, et al. 2002. Eventual AIDS vaccine failure in a rhesus monkey by viral escape from cytotoxic T lymphocytes. *Nature* 415: 335–339.
26. O'Connor, D. H., B. R. Mothe, J. T. Weinfurter, S. Fuenger, W. M. Rehrauer, P. Jing, R. R. Rudersdorf, M. E. Liebl, K. Krebs, J. Vasquez, et al. 2003. Major histocompatibility complex class I alleles associated with slow simian immunodeficiency virus disease progression bind epitopes recognized by dominant acute-phase cytotoxic-T-lymphocyte responses. *J. Virol.* 77: 9029–9040.
27. Dandekar, A. A., G. Jacobsen, T. J. Waldschmidt, and S. Perlman. 2003. Antibody-mediated protection against cytotoxic T-cell escape in coronavirus-induced demyelination. *J. Virol.* 77: 11867–11874.
28. Kim, T. S., and S. Perlman. 2003. Protection against CTL escape and clinical disease in a murine model of virus persistence. *J. Immunol.* 171: 2006–2013.
29. Pewe, L., S. Xue, and S. Perlman. 1997. Cytotoxic T-cell-resistant variants arise at early times after infection in C57BL/6 but not in SCID mice infected with a neurotropic coronavirus. *J. Virol.* 71: 7640–7647.
30. Weiss, S. R., and S. Navas-Martin. 2005. Coronavirus pathogenesis and the emerging pathogen severe acute respiratory syndrome coronavirus. *Microbiol. Mol. Biol. Rev.* 69: 635–664.
31. Leslie, A. G. W. 1992. Recent changes to the MOSFLM package for processing film and image plate data. In *CCP4 and ESF-EAMCB Newsletter on Protein Crystallography*, No. 26. Daresbury Laboratory, Warrington.
32. Evans, P. R. 1992. Data reduction: data collection and processing. In *Proceedings of the CCP4 study weekend. Data collection and processing.* eds. L. Sawyer, N. W. Isaacs, and S. Bailey. Daresbury Laboratory, Warrington. pp. 114–122.
33. Storoni, L. C., A. J. McCoy, and R. J. Read. 2004. Likelihood-enhanced fast rotation functions. *Acta Crystallogr. D Biol. Crystallogr.* 60: 432–438.
34. Murshudov, G. N., A. A. Vagin, and E. J. Dodson. 1997. Refinement of macromolecular structures by the maximum-likelihood method. *Acta Crystallogr. D Biol. Crystallogr.* 53: 240–255.
35. Emsley, P., and K. Cowtan. 2004. Coot: model-building tools for molecular graphics. *Acta Crystallogr. D Biol. Crystallogr.* 60: 2126–2132.
36. Lamzin, V. S., and K. S. Wilson. 1993. Automated refinement of protein models. *Acta Crystallogr. D Biol. Crystallogr.* 49: 129–147.
37. Kuo, L., G. J. Godeke, M. J. Raamsman, P. S. Masters, and P. J. Rottier. 2000. Retargeting of coronavirus by substitution of the spike glycoprotein ectodomain: crossing the host cell species barrier. *J. Virol.* 74: 1393–1406.
38. Anghelina, D., L. Pewe, and S. Perlman. 2006. Pathogenic role for virus-specific CD4 T cells in mice with coronavirus-induced acute encephalitis. *Am. J. Pathol.* 169: 209–222.
39. Perlman, S., R. Schelper, E. Bolger, and D. Ries. 1987. Late onset, symptomatic, demyelinating encephalomyelitis in mice infected with MHV-JHM in the presence of maternal antibody. *Microb. Pathog.* 2: 185–194.
40. Ogino, S., T. Kawasaki, M. Brahmandam, L. Yan, M. Cantor, C. Namgyal, M. Mino-Kenudson, G. Y. Lauwers, M. Loda, and C. S. Fuchs. 2005. Sensitive sequencing method for *KRAS* mutation detection by Pyrosequencing. *J. Mol. Diagn.* 7: 413–421.
41. Hamilton, S. E., and J. T. Harty. 2002. Quantitation of $CD8^+$ T cell expansion, memory, and protective immunity after immunization with peptide-coated dendritic cells. *J. Immunol.* 169: 4936–4944.
42. Wu, G. F., A. A. Dandekar, L. Pewe, and S. Perlman. 2000. CD4 and CD8 T cells have redundant but not identical roles in virus-induced demyelination. *J. Immunol.* 165: 2278–2286.
43. Rognan, D., L. Scapozza, G. Folkers, and A. Daser. 1995. Rational design of nonnatural peptides as high-affinity ligands for the HLA-B*2705 human leukocyte antigen. *Proc. Natl. Acad. Sci. USA* 92: 753–757.
44. Webb, A. I., N. A. Borg, M. A. Dunstone, L. Kjer-Nielsen, T. Beddoe, J. McCluskey, F. R. Carbone, S. P. Bottomley, M. I. Aguilar, A. W. Purcell, and J. Rossjohn. 2004. The structure of H-$2K^b$ and K^{bm8} complexed to a herpes simplex virus determinant: evidence for a conformational switch that governs T cell repertoire selection and viral resistance. *J. Immunol.* 173: 402–409.
45. Webb, A. I., M. A. Dunstone, N. A. Williamson, J. D. Price, A. de Kauwe, W. Chen, A. Oakley, P. Perlmutter, J. McCluskey, M. I. Aguilar, et al. 2005. T cell determinants incorporating β-amino acid residues are protease resistant and remain immunogenic in vivo. *J. Immunol.* 175: 3810–3818.
46. Ljunggren, H. G., N. J. Stam, C. Ohlen, J. J. Neefjes, P. Hoglund, M. T. Heemels, J. Bastin, T. N. Schumacher, A. Townsend, K. Karre, et al. 1990. Empty MHC class I molecules come out in the cold. *Nature* 346: 476–480.
47. Klenerman, P., and R. M. Zinkernagel. 1998. Original antigenic sin impairs cytotoxic T lymphocyte responses to viruses bearing variant epitopes. *Nature* 394: 482–485.
48. Achour, A., J. Michaelsson, R. A. Harris, J. Odeberg, P. Grufman, J. K. Sandberg, V. Levitsky, K. Karre, T. Sandalova, and G. Schneider. 2002. A structural basis for LCMV immune evasion: subversion of H-$2D^b$ and H-$2K^b$ presentation of gp33 revealed by comparative crystal structure analyses. *Immunity* 17: 757–768.
49. Leslie, A. J., K. J. Pfafferott, P. Chetty, R. Draenert, M. M. Addo, M. Feeney, Y. Tang, E. C. Holmes, T. Allen, J. G. Prado, et al. 2004. HIV evolution: CTL escape mutation and reversion after transmission. *Nat. Med.* 10: 282–289.
50. Crawford, H., J. G. Prado, A. Leslie, S. Hue, I. Honeyborne, S. Reddy, M. van der Stok, Z. Mncube, C. Brander, C. Rousseau, et al. 2007. Compensatory mutation partially restores fitness and delays reversion of escape mutation within the immunodominant HLA-B*5703-restricted Gag epitope in chronic human immunodeficiency virus type 1 infection. *J. Virol.* 81: 8346–8351.
51. Yeh, W. W., E. M. Cale, P. Jaru-Ampornpan, C. I. Lord, F. W. Peyerl, and N. L. Letvin. 2006. Compensatory substitutions restore normal core assembly in simian immunodeficiency virus isolates with Gag epitope cytotoxic T-lymphocyte escape mutations. *J. Virol.* 80: 8168–8177.
52. Turner, S. J., K. Kedzierska, H. Komodromou, N. L. La Gruta, M. A. Dunstone, A. I. Webb, R. Webby, H. Walden, W. Xie, J. McCluskey, et al. 2005. Lack of prominent peptide-major histocompatibility complex features limits repertoire diversity in virus-specific $CD8^+$ T cell populations. *Nat. Immunol.* 6: 382–389.
53. Pewe, L. L., J. M. Netland, S. B. Heard, and S. Perlman. 2004. Very diverse CD8 T cell clonotypic responses after virus infections. *J. Immunol.* 172: 3151–3156.
54. Pewe, L., S. B. Heard, C. Bergmann, M. O. Dailey, and S. Perlman. 1999. Selection of CTL escape mutants in mice infected with a neurotropic coronavirus: quantitative estimate of TCR diversity in the infected central nervous system. *J. Immunol.* 163: 6106–6113.
55. Fleming, J. O., M. D. Trousdale, F. A. el-Zaatari, S. A. Stohlman, and L. P. Weiner. 1986. Pathogenicity of antigenic variants of murine coronavirus JHM selected with monoclonal antibodies. *J. Virol.* 58: 869–875.
56. Jacobsen, G., and S. Perlman. 1990. Localization of virus and antibody response in mice infected persistently with MHV-JHM. *Adv. Exp. Med. Biol.* 276: 573–578.
57. Parker, S. E., T. M. Gallagher, and M. J. Buchmeier. 1989. Sequence analysis reveals extensive polymorphism and evidence of deletions within the E2 glycoprotein gene of several strains of murine hepatitis virus. *Virology* 173: 664–673.
58. Phillips, J. J., M. M. Chua, G. F. Rall, and S. R. Weiss. 2002. Murine coronavirus spike glycoprotein mediates degree of viral spread, inflammation, and virus-induced immunopathology in the central nervous system. *Virology* 301: 109–120.
59. Wang, F. I., D. R. Hinton, W. Gilmore, M. D. Trousdale, and J. O. Fleming. 1992. Sequential infection of glial cells by the murine hepatitis virus JHM strain (MHV-4) leads to a characteristic distribution of demyelination. *Lab. Invest.* 66: 744–754.
60. Tsai, J. C., B. D. Zelus, K. V. Holmes, and S. R. Weiss. 2003. The N-terminal domain of the murine coronavirus spike glycoprotein determines the CEACAM1 receptor specificity of the virus strain. *J. Virol.* 77: 841–850.
61. Bergmann, C. C., J. D. Altman, D. Hinton, and S. A. Stohlman. 1999. Inverted immunodominance and impaired cytolytic function of $CD8^+$ T cells during viral persistence in the central nervous system. *J. Immunol.* 163: 3379–3387.
62. Ramakrishna, C., R. A. Atkinson, S. A. Stohlman, and C. C. Bergmann. 2006. Vaccine-induced memory $CD8^+$ T cells cannot prevent central nervous system virus reactivation. *J. Immunol.* 176: 3062–3069.
63. Day, C. L., D. E. Kaufmann, P. Kiepiela, J. A. Brown, E. S. Moodley, S. Reddy, E. W. Mackey, J. D. Miller, A. J. Leslie, C. DePierres, et al. 2006. PD-1 expression on HIV-specific T cells is associated with T-cell exhaustion and disease progression. *Nature* 443: 350–354.
64. Moskophidis, D., F. Lechner, H. Hengartner, and R. M. Zinkernagel. 1994. MHC class I and non-MHC-linked capacity for generating an anti-viral CTL response determines susceptibility to CTL exhaustion and establishment of virus persistence in mice. *J. Immunol.* 152: 4976–4983.
65. Moskophidis, D., F. Lechner, H. Pircher, and R. M. Zinkernagel. 1993. Virus persistence in acutely infected immunocompetent mice by exhaustion of antiviral cytotoxic effector T cells. *Nature* 362: 758–761.
66. Robinson, H. L. 2003. T cells versus HIV-1: fighting exhaustion as well as escape. *Nat. Immunol.* 4: 12–13.
67. Barber, D. L., E. J. Wherry, D. Masopust, B. Zhu, J. P. Allison, A. H. Sharpe, G. J. Freeman, and R. Ahmed. 2006. Restoring function in exhausted CD8 T cells during chronic viral infection. *Nature* 439: 682–687.
68. Velu, V., S. Kannanganat, C. Ibegbu, L. Chennareddi, F. Villinger, G. J. Freeman, R. Ahmed, and R. R. Amara. 2007. Elevated expression levels of inhibitory receptor programmed death 1 on simian immunodeficiency virus-specific CD8 T cells during chronic infection but not after vaccination. *J. Virol.* 81: 5819–5828.
69. Shao, L., H. Shinzawa, X. Zhang, D. B. Smith, H. Watanabe, H. Mitsuhashi, K. Saito, T. Saito, H. Togashi, and T. Takahashi. 2000. Diversity of hepatitis G virus within a single infected individual. *Virus Genes* 21: 215–221.